33. Sakano, H., Maki, R., Kurosawa, Y., Roeder, W. & Tonegawa, S. *Nature* **286,** 676-683 (1983).
34. Breathnach, R. & Chambon, P. *A. Rev. Biochem.* **50,** 349-383 (1981).
35. Samelson, L. E., Germain, R. N. & Schwartz, R. H. *Proc. natn. Acad. Sci. U.S.A.* **80,** 6972-6976 (1983).
36. Van den Elsen, P. *et al. Nature* **312,** 413-418 (1984).
37. Gold, D. P. *et al. Nature* **321,** 431-434 (1986).
38. Krissansen, G. W., Owen, M. J., Verbi, W. & Crumpton, M. J. *EMBO J.* **5,** 1799-1808 (1986).
39. Zlotnik, A. *et al. Proc. natn. Acad. Sci. U.S.A.* (in the press).
40. Snodgrass, H. R., Dembic, Z., Steinmetz, M. & von Boehmer, H. *Nature* **315,** 232-233 (1985).
41. Raulet, D. H., Garman, R. D., Saito, H. & Tonegawa, S. *Nature* **314,** 103-107 (1985).
42. Samelson L. E. *et al. Nature* **315,** 765-768 (1985).
43. Reth, M. G. & Alt, F. W. *Nature* **312,** 418-423 (1984).
44. Kavaler, J., Davis, M. M. & Chien, Y. *Nature* **310,** 421-423 (1984).
45. Siu, G. *et al. Nature* **311,** 344-350 (1984).
46. Rupp, F., Frech, G., Hengartner, H., Zinkernagel, R. M. & Joho, R. *Nature* **321,** 876-878 (1986).
47. Reilly, E. B., Kranz, K. M., Tonegawa, S. & Eisen, H. N. *Nature* **321,** 876-878 (1986).
48. Traunecker, A., Oliveri, F., Allen, N. & Karjalainen, K. *EMBO J.* **5,** 1589-1593 (1986).
49. Zauderer, M., Iwamato, A. & Mak, T. W. *J. exp. Med.* **163,** 1314-1318 (1986).
50. Heiter, P. A., Korsmeyer, S. J., Waldmann, T. A. & Leder, P. *Nature* **290,** 368-372 (1981).
51. Honjo, T. & Kataoka, T. *Proc. natn. Acad. Sci. U.S.A.* **75,** 2140-2144 (1978).
52. Davis, M. M. *et al. Nature* **283,** 733-739 (1980).
53. Blattner, F. R. & Tucker, P. N. *Nature* **307,** 417-422 (1984).
54. Cory, S., Graham, M., Webb, E., Corcoran, L. & Adams, J. *EMBO J.* **4,** 675-681 (1985).
55. Feinberg, A. & Vogelstein, B. *Analyt. Biochem.* **132,** 6-13 (1983).
56. Chen, E. Y. & Seeburg, P. H. *DNA* **4,** 165-170 (1985).
57. Henikoff, S. *Gene* **28,** 351-359 (1984).
58. Hayday, A. C. *et al. Cell* **40,** 259-269 (1985).
59. Gascoigne, N. R. J., Chien, Y., Becker, D. M., Kavaler, J. & Davis, M. M. *Nature* **310,** 387-391 (1984).
60. Kabat, E. A., Wu, T. T., Reid-Miller, M., Perry, H. & Gottesman, K. S. *U.S. Dept. Health and Human Services* (1987).

LETTERS TO NATURE

Neutrino temperatures and fluxes from the LMC supernova

J. N. Bahcall, T. Piran*‡, W. H. Press†‡ & D. N. Spergel

The Institute for Advanced Study, Princeton, 08540, USA
* RACAH Institute for Physics, Hebrew University, Jerusalem, Israel
† Department of Astronomy, Harvard University, Cambridge, Massachusetts 02138, USA

The observation[1,2] of neutrinos from the LMC supernova makes possible direct tests of the theory of supernova explosions and of properties of weakly interacting particles. Here we describe a combined analysis of the angular and energy distributions of the events observed in the Kamiokande and the IMB detectors which determines the effective temperatures and fluxes of neutrinos and anti-neutrinos produced by the explosion. Our main result is that a simple model is consistent with the available data and in reasonable agreement with conventional models of supernova explosions. The parameters of the model are: a single temperature, T, of $4.1^{+1.0}_{-0.4}$ MeV, a flux of electron anti-neutrinos of $(0.5^{+0.2}_{-0.35})\times 10^{10}$ cm^{-2} [total energy in $\bar{\nu}_e = (3.0^{+1.7}_{-1.4}\times 10^{52}$ erg)], and a poorly determined flux of 'scattered' (see below) neutrinos = $(0.2\text{–}5)\times 10^{10}$ cm^{-2}. Several statistical tests were used to determine the acceptable range of these parameters. We have also set limits on possible high-temperature fluxes of neutrinos or anti-neutrinos that might result from matter oscillations[3,4].

The dominant events in both the Kamiokande (2.1 active ktons) and the IMB (5 active ktons) water detectors are expected[1,2,5] to be the absorption of electron anti-neutrinos by protons and the scattering of neutrinos of all flavours by electrons. The experimental quantities that we use are the measured energies and angles (with which the detected electron or positron moves relative to the direction of the LMC) of each of the events, together with their quoted 1σ uncertainties. The IMB collaboration, with a threshold just below 20 MeV, observed 8 events with energies between 20 MeV and 44 MeV. The Kamiokande II collaboration (threshold ~7 MeV) reported 11 events spread out over 12.4 seconds. The first 8 events occurred within <2 s and were followed by a 7-s gap. The subsequent three events, with lower average energy, could have been generated by a process with different parameters. One might be tempted to speculate that these latter events correspond to scattering of electrons by mu or tau neutrinos (or other exotic particles) with a rest mass of ~20 eV (to explain the time delay). This speculation can be ruled out at the 99.7% confidence level because the events in question make relatively large angles with respect to the direction to the LMC (122°±30°, 49°±26° and 91°±39°.)

‡ Present address: Institute for Advanced Study, Princeton, New Jersey 08540, USA

The detection of two events in the IMB detector during the gap in the Kamiokande detector reduces the significance of the gap. In a subsequent paper[6], we show that a thermal spectrum from a cooling neutron star describes well the arrival times as well as the observed energies. Since the neutron star probably cooled significantly by the time (~10 s) the last Kamiokande events were observed, we concentrate our single temperature analysis on the first 10 seconds.

We shall consider first solutions in which each type of neutrino (i = electron, muon, tau, and their anti-neutrinos) is decribed by a thermal spectrum, with an associated temperature, T_i, and a flux, F_i at Earth (measured per cm^2). The rate at which events of a definite energy (E_e) are observed in each detector can be written

$$R(E_e,\{T_i, F_i\}) = \sum_{i,j} F_i N_j \int\int dE'_e dq (d\sigma_j/dE'_e)_i \times \phi_i(q, T_i)\varepsilon(E'_e)g(E_e, E'_e, \sigma'_e)$$

where we denote the various neutrino temperatures and fluxes by $\{T_i, F_i\}$, the energy of the electron (or positron) that is produced by E_e, the neutrino energy by q, the neutrino interaction cross sections by $d\sigma_j/dE (j = 1, 2$ for scattering and absorption), the neutrino spectrum by $\phi \propto q^2 \exp(-q/T)$, the detection efficiency by ε, and the measuring error by g (which we represent in practice by a gaussian). We have linearly interpolated between the reported[1,2] detection efficiencies to obtain simple representations of the detection efficiencies, ε.

The absorption cross-section is approximately quadratic in energy: $\sigma_{abs} = 8.9\times 10^{-42}$ cm^2 $(E'/10$ MeV$)^2$. The scattering cross-sections are more complicated; in the calculations described below, we have used the full expressions[7]. The following approximation, $(d\sigma_{scatt}/dE')dE' = \text{constant}\times 10^{-44}$ cm^2 $(dE'/10$ MeV), is useful in interpreting the results. For ν_e-e ν_μ-e, $\bar{\nu}_e$-e and $\bar{\nu}_\mu$-e scattering, the constant is, respectively, 9.2 1.6, 3.9 and 1.3. The total scattering cross-sections are represented, for the energies of interest here, to an accuracy of ~10% by the approximation given above. We have also included contributions from neutrino absorption by oxygen, which, however, is unimportant at the temperatures considered here.

The corresponding formula for the angular distribution is (μ is the cosine of the angle that the recoil electron or positron makes with respect to the direction of the LMC):

$$A(\mu,\{T_i, F_i\})\, d\mu = \sum_{i,j} F_i N_j\, d\mu \int\int d\mu'\, dq (d\sigma_j/d\mu')_i \times \phi_i(q, T_i)\varepsilon(E_e)S(\mu, \mu') \quad (2)$$

where the smoothing function S represents the uncertainty of the angular measurements, $S \propto \sin\theta' \exp(-\theta_b^2/\Delta(\theta')^2)$ and θ_b is the angle between the measured direction (represented by μ) and the actual direction (represented by μ') in which the electron moves. The absorption events are nearly isotropic: probability

$P(\mu')\,d\mu' = d\mu'[1-0.10(v/c)\mu']$, where v is the velocity of the produced positron. The scattering cross-section is, on the other hand, strongly forward peaked (see equations (9) and (20) of ref. 7 for the detailed formulae we have used). The IMB detector was biased against backscattering events during the period when the supernova was detected; we included this bias by setting the efficiency for detection equal to 1.0/1.15 for $\mu < 0$.

The functions representing the experimental errors (g in equation (1) and S in equation (2)) are very important since the energy distributions (and interaction cross-sections) of the incoming neutrinos are not flat and the scattering cross-section is strongly forward peaked. Measuring errors shift the apparent energy distribution of events in the IMB detector to significantly higher energies for the inferred anti-neutrino temperatures discussed below. For our preferred temperature (see equation (3a) below), including the measurement errors in energy increases the expected number of events in the IMB detector that are seen to be above 35 MeV by 50% and doubles the total number of events above 40 MeV.

We can at best determine one flux of 'average' scatterers. At the energies considered here, electron, muon or tau neutrinos (or anti-neutrinos) will all scatter electrons in the forward direction. We do not have any way of separating, in a model-independent way, neutrinos and anti-neutrinos of different flavours from their electron neutrino counterparts. For the conventional fluxes and temperatures summarized in Table 1 of ref. 5 and the scattering cross-sections given above, $\sum_i \text{Flux (i)}\sigma_{\text{scatt}}\text{(i)} \approx 1.6\ \text{Flux}\ (\nu_e)\sigma_{\text{scatt}}(\nu_e)$. In what follows, we lump together the fluxes of all neutrino and anti-neutrino scatterers into an 'effective' scattering flux, F_{scatt} defined by $F_{\text{scatt}}\sigma_{\text{scatt}}\ (\nu_e) \equiv \sum_i \text{Flux (i)}\sigma_{\text{scatt}}\ \text{(i)}$. We expect, but cannot prove, that $F_{\nu_e} \sim 0.5 \times F_{\text{scatt}}$.

Most (but not all) of the information regarding the temperatures is contained in the measured energy distributions; most (but not all) of the information regarding the ratio of ν_{scatt} to $\bar{\nu}_e$ fluxes is contained in the measured angular distributions. The reader can readily appreciate the coupled nature of the problem by considering the following example. The forward peaking observed in the Kamiokande detector (five events within 45° of the LMC direction) suggests an appreciable amount of ν-e scattering, while the relatively isotropic IMB data indicate that, at the higher energies observed in this detector, scattering is not particularly important. The absorption cross-section increases more rapidly with energy than the scattering cross-section (see above); this fact is related to both the relative number of events observed in the two detectors and their different angular distributions. The strongest limits on $F_{\text{scatt}}/F_{\bar{\nu}_e}$ result from the relative isotropy of the IMB events combined with the forward peaking observed in Kamiokande.

We have performed both estimation-of-parameters and goodness-of-fit tests on the data. Maximum likelihood parameters were estimated using a single likelihood function that incorporates the expected energy and angular distributions, as well as the quoted[1,2] detector efficiencies and measurement errors in each detector. The joint likelihood function also takes into account the absolute number of events in each detector. Use of a joint likelihood function gives parameters that are most consistent with the observations in both detectors. To test whether this consistency is credible, without reference to likelihood, we find the range of parameters allowed by the Kolmogorov-Smirnov (KS) measures of the goodness-of-fit to the observed energies and angles of the individual events. Finally, we have also verified that the maximum likelihood and KS tests are consistent by doing Monte Carlo simulations with the maximum likelihood parameter values. The simulations do indeed produce synthetic data sets that are strongly concentrated in the KS-allowed region.

Figure 1 shows our results for the allowed range of T and $F_{\text{scatt}}/F_{\bar{\nu}_e}$. The star marks the peak of the likelihood function. Solid contours indicate where the likelihood function is 0.1 and 0.01 of the peak value. Different aspects of the data rule out separate parts of the parameter plane. Darker shades delineate regions that are excluded by data from both experiments. The region outside the short dashed lines is excluded (less than 5% significance level) for the KS measure of the energy distribution of the Kamiokande data. Similarly the region outside the long dashed lines is excluded by the KS measure of the energy distribution of the IMB data. The KS measure of the angular distribution of the Kamiokande data rules out (again with 5% significance) the region above the dotted line. The allowed region (dashed lines) is determined on the high-temperature side by the energy distribution measured in the Kamiokande detector and on the low-temperature side by the IMB energies.

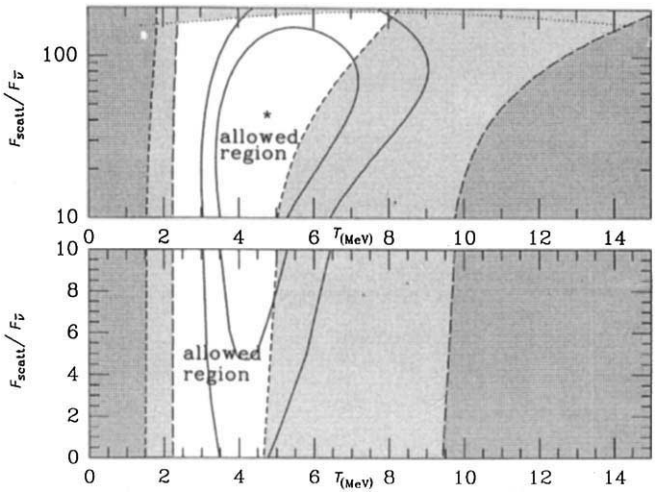

Fig. 1 Allowed and excluded temperatures: the allowed regions are unshaded and the excluded regions are shaded. Contours of the joint likelihood function are indicated by the smooth curves in the T, $F_{\text{scatt}}/F_{\bar{\nu}_e}$ plane. Darker regions are excluded by both detectors. The region outside the long dashed lines is excluded by the energy distribution of the IMB data (at 0.05 significance with a Kolmogorov–Smirnov test). The region outside the short dashed lines is excluded by the energy distribution of the Kamiokande data (at 0.05 significance). The region above the dotted line is excluded by the angular distribution of the Kamiokande data (at 0.05 significance). The overall allowed region is bounded by the upper limits to the temperature from the Kamiokande data, and by the lower limits to the temperature from the IMB data. The solid lines indicate contours of the likelihood function at 10% (inner) and 1% (outer) of its maximal value. While the upper half of the plot is not excluded by the observed data, it is unlikely on the basis of energy considerations (see discussion preceding equation 3(c)). The shadings shown here do not depend upon the relative sensitivity of the detectors.

The ratio of scattered events in Kamiokande to absorption events in IMB sets another temperature-dependent limit on $F_{\text{scatt}}/F_{\bar{\nu}_e}$ which rules out high values of $F_{\text{scatt}}/F_{\bar{\nu}_e}$ at low temperatures. Finally, the ratio of the number of absorption events in the two detectors sets a lower limit of 3.7 MeV for the temperature (see Fig. 2*a*).

The formal maximum of the likelihood function occurs at $T = 4.8$ MeV, $F_{\text{scatt}}/F_{\bar{\nu}_e} = 44$, and $F_{\bar{\nu}_e} = 0.25 \times 10^{10}\ \text{cm}^{-2}$. This high value of $F_{\text{scatt}}/F_{\bar{\nu}_e}$ is, however, physically unreasonable; it corresponds to $F_{\text{scatt}} = 11 \times 10^{10}\ \text{cm}^{-2}$ and therefore would imply that much more than 0.1 $M_\odot$ was radiated in neutrinos (see remarks regarding total energy that precede equation (3c)). The likelihood function is also consistent with smaller values of $F_{\text{scatt}}/F_{\bar{\nu}_e} \leq 10$. For these physically plausible values of the flux ratio, the 'ridge line' (maximum of the likelihood function as T varies at a fixed flux ratio) lies nearly along the constant value

$$T = 4.1\ \text{MeV}. \qquad (3a)$$

The corresponding value of $F_{\bar{\nu}_e}$ is $0.5 \times 10^{10}\ \text{cm}^{-2}$. If we include the last three events in the Kamiokande data, the maximal

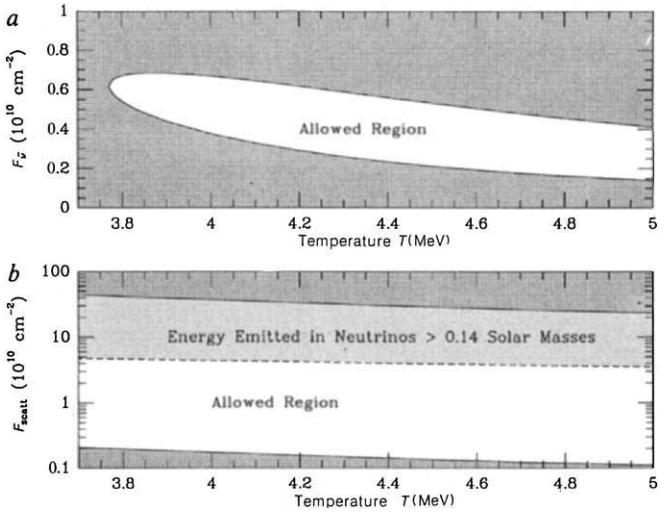

Fig. 2 *a*, Allowed range of anti-neutrino fluxes: electron anti-neutrino fluxes between the solid lines are consistent (5% significance) with the detection of between 3 and 7 anti-neutrino absorbtion events in Kamiokande and between 6 and 8 absorption events in the IMB. *b*, Allowed range of scattering neutrino fluxes: neutrino fluxes between the solid lines are consistent (5% significance) with the detection of between 1 and 5 scattering events in Kamiokande and 0 to 2 scattering events in IMB. Fluxes above the dashed line correspond to an emitted energy in neutrinos that exceeds the binding energy of a neutron star.

allowed temperature (as determined by the Kamiokande data) is reduced to 3.5 MeV (for $F_{\text{scatt}}/F_{\bar{\nu}_e} < 10$). While this result is consistent with the lower range of the IMB data (see Fig. 1), it reduces significantly the calculated likelihood of the combined data. A better fit to the last three data points can be obtained by assuming that the neutron star is cooling, which naturally leads to a lower temperature producing the later points[6].

The single temperature model represents a satisfactory fit to the observations. For $T = 4.1$ MeV and $F_{\text{scatt}}/F_{\bar{\nu}_e} = 10$, the probability of obtaining a worse KS measure than was found for the observed energy distribution is 33% for the Kamiokande data and 65% for the IMB data.

Monte Carlo simulations show that (5% significance) between 3 and 7 of the first 8 events in Kamiokande were due to absorption of electron anti-neutrinos. The KS test can only reject the possibility of 0 scattering events at 2% significance, which is small but not completely negligible. There were between 6 and 8 absorption events in IMB (95% confidence level).

Figure 2*a* shows that there is a well-defined range of anti-neutrino fluxes,

$$F_{\bar{\nu}_e} = (0.15\text{–}0.7) \times 10^{10}\ \text{cm}^{-2} \qquad (3b)$$

(95% confidence level) that is consistent with both the observed event rates. If we require that the count rates in IMB and Kamiokande are compatible and assume that the detector efficiencies are accurately known[1,2], then the neutrino temperature must exceed 3.7 MeV.

For the temperature and flux ranges inferred here (equations (3a) and (3b)), we would not expect a large signal in either the Mont Blanc or the Baksan scintillator detectors[8]. Assuming a detection efficiency of 100%, we estimate $0.8 \times (T/4.1\ \text{MeV})^2 (F_{\bar{\nu}_e}/0.5 \times 10^{10}\ \text{cm}^{-2})$ absorption events per 100 metric tons of scintillator.

As was already seen from Fig. 1, a much larger range is acceptable for the flux of ν_{scatt}, which is determined by a small number of events in the forward peak of either detector. The ν_{scatt} flux is harder to determine than the $\bar{\nu}_e$ flux because the scattering cross-section is much smaller than the absorption cross-section.

The strongest experimental limit on F_{scatt} comes from the detection of one to five (forward-peaked) scattering events in Kamiokande (see discussion of Monte Carlo experiments preceding Fig. 2*a*). The likelihood function does not vary significantly over this range but is peaked between two and three scattering events. Figure 2*b* shows that there is a large range of fluxes consistent at the 95% confidence level with one to five scattering events in Kamiokande. All fluxes in this range are consistent with the detection of 0 to 2 scattering events in IMB.

The formation of a neutron star in a type II supernova is expected to relase, in neutrinos, nearly all of the star's binding energy, $0.1 \times M_{\text{neutron star}}$, which is 2.6×10^{53} ergs for a neutron star of mass 1.4 $M_\odot$. Requiring that the energy emitted in neutrinos does not exceed the energy released by the collapse of the core to form a neutron star further constrains F_{scatt}. The total energy, E_{total},that is removed by neutrinos is $E_{\text{total}} = 5.9 \times 10^{52}\ \text{erg}\ (F/10^{10}\ \text{cm}^{-2})\ (T/4.1\ \text{MeV})\ (D/50\ \text{kpc})^2$. The region above the dashed line in Fig. 2*b* corresponds to a total emitted neutrino energy in excess of 3×10^{53} ergs. We adopt as the acceptable range,

$$F_{\text{scatt}} = (0.1\text{–}5) \times 10^{10}\ \text{cm}^{-2} \qquad (3c)$$

The upper limit in equation (3*c*) could be increased slightly if we assumed that the supernova produced a neutron star more massive than 1.44 $M_\odot$, which subsequently cooled and collapsed to form a black hole.

Can the expected flux of ν_e be detected in the ^{37}Cl experiment of Davis? The calculated number of events occurring in the ^{37}Cl tank, corresponding to the range of fluxes given in equation (3c), varies from 0.02 to 2, depending upon whether one uses the upper limit (with $F(\nu_e) = F_{\text{scatt}}$) or the lower limit (with $F(\nu_e) = 0.5 \times F_{\text{scatt}}$). The background from solar neutrinos will probably be too large to permit a stringent test of equation (3c).

The mass of $\bar{\nu}_e$ is strongly constrained[9] by the observed energies and arrival times of the lowest-energy neutrino events if these events are due to absorption and not scattering (otherwise, the kinematic relations are not unique). The most important event has the lowest energy, 7.5 MeV, and is observed at an angle of $108° \pm 32°$ with respect to the LMC; the probability that this event is due to scattering is $<0.2\%$. The two next most important events have measured energies 9.2 MeV ($70° \pm 30°$) and 12.8 MeV ($135° \pm 23°$); the corresponding probabilities that these events are due to scattering are, respectively, 5% and $\ll 0.1\%$. We conclude that it is valid to use absorption kinematics in constraining the mass of $\bar{\nu}_e$.

We now consider the following question: is there any evidence for or against matter oscillations of neutrinos (the MSW effect[3,4]) having affected the neutrino fluxes or spectra? Yes, provided we consider the unfamiliar case in which the electron's neutrino is predominantly associated with the highest mass eigenstate. The ν_μ and ν_τ and their anti-neutrinos, are expected on conventional supernova models (see, for example, Table 1 of ref. 5) to be produced in comparable numbers to ν_e and $\bar{\nu}_e$, but with a temperature that may be a factor of two higher ($\sim$10 MeV). The key point is that the higher-temperature mu and tau anti-neutrinos can, for the unconventional mass hierarchy we stress here, be converted to more easily observable electron anti-neutrinos by neutrino oscillations.

If, on the other hand, the mixing angles are all small and the lowest mass eigenstate is almost pure ν_e, matter oscillations constitute an attractive solution[3] of the solar neutrino problem, one that is consistent with some grand unified theories. However, as pointed out earlier in a prescient study[9], the expected effects on supernova neutrinos are not large for matter oscillations satisfying the above assumptions. Wolfenstein[10] has noted that large mixing angles are also possible and may, for certain parameters, both solve the solar neutrino problem and have appreciable effects on the observed supernova neutrino spectra and fluxes.

What limits can be placed on possible high-temperature components of $\nu_{scatter}$ and $\bar{\nu}_e$? From the total number of events observed in the IMB detector, we find that the upper limit (95% confidence level) on the number of high temperature, $T > 10$ MeV, neutrinos is

$$F_{\bar{\nu}_e}(T > 10\ \text{MeV}) \leq 0.1 \times 10^{10}\ \text{cm}^{-2}\ (10\ \text{MeV}/T) \quad (4a)$$

and, from the angular distribution of the IMB events and the total energy constraint (see discussion preceding equation (3c)

$$F_{\text{scatt}}(T > 10\ \text{MeV}) \leq 2 \times 10^{10}\ \text{cm}^{-2}(10\ \text{MeV}/T) \quad (4b)$$

But if matter oscillations with large mixing angles do occur and $\bar{\nu}_e$, $\bar{\nu}_\mu$ and $\bar{\nu}_\tau$ were produced in comparable numbers, then one might expect to have observed a high-temperature component of $\bar{\nu}_e$ that represented converted mu and tau anti-neutrinos. As both $\bar{\nu}_\mu$ and $\bar{\nu}_\tau$ could have been converted to $\bar{\nu}_e$, favourable conditions would have resulted in a flux of about twice as many (converted) high temperature $\bar{\nu}_e$ as direct low-temperature $\bar{\nu}_e$. Equation (4a) shows that this did not occur. In fact, this conceivable manifestation of the MSW effect did not occur at a level of 0.1 or more above what might have been expected.

Our main conclusions are summarized below. (1) The temperatures and fluxes (equations (3a-c)) inferred here are in remarkable agreement with the standard theoretical ideas of how stars collapse and supernovae are formed[11-21]; the observations of supernova neutrinos represent therefore a great triumph for astrophysical theory. Table 1 of ref. 5 gives a convenient summary of the (pre-observation) expectations. The numerical comparison between observations (equation (3)) and expectations (Table 1 of ref. 5) is: $T_{\text{expect}} = 5$ MeV $[T_{\text{obs}} = 4.1^{+1.0}_{-0.4}$ MeV]; $F_{\text{expect}} = 1.1 \times 10^{10}\ \text{cm}^{-2}$; $[F_{\text{obs}} = 0.5^{+0.2}_{0.35} \times 10^{10}\ \text{cm}^{-2}]$; and $F_{\text{expect}}(\nu_e) = 1.6 \times 10^{10}\ ^{c}\text{m}^{-2}$ $[F_{\text{obs}}(\text{scatt}) = (0.1\text{-}5) \times 10^{10}\ \text{cm}^{-2}]$. The total energy in neutrinos is, within the uncertainties, consistent with the theoretical expectation of 3×10^{53} ergs. This model suggests that the full (3 kton) Kamiokande detector experienced $\sim 20(T/4.1\ \text{MeV})^2(\text{Flux}/0.5 \times 10^{10}\ \text{cm}^{-2})$ absorption events (assuming 100% efficiency). (2) The simplest (one-temperature thermal) model provides an acceptable fit to the observed energy and angular distributions of both the Kamiokande and the IMB observations. The success of the simple model means that major refinements are not required by the data, except perhaps to explain the three delayed events observed in the Kamiokande detector[6]. One can use the observations to rule out more detailed and specific astrophysical models, but it seems unlikely that one will be able to infer many additional parameters in an unambiguous fashion. (3) Between 3 and 7 absorption events were observed in Kamiokande and between 6 and 8 absorption events were detected by IMB (5% significance). The possibility of zero scattering events in both detectors can only be rejected at the level of 2% significance. The crucial low-energy events, which are important for setting an upper limit on the mass of $\bar{\nu}_e$, can safely be ascribed to absorption, not scattering. (4) We expect[5] only a small number of events in the Mont Blanc, Baksan and Homestake (^{37}Cl) detectors. (5) The observations constrain possible high-temperature neutrino fluxes (see equation (4)), and argue against the occurrence of the MSW effect in an unconventional mass hierarchy in which electron neutrinos are predominantly associated with the heaviest mass eigenstates.

While this work was being completed, we received several interesting and relevant papers (J. Arafune and S. Fukujita, preprint RIFP-693, Kyoto University, 1987, K. Sato and H. Suzaki, UTAP-47, University of Tokyo, 1987; refs 22, 23). Our paper is the first joint statistical analysis of the result in both the Kamiokande and the IMB experiments, which accounts for the fact that some of our conclusions are different from those given in the recent preprints.

We thank the Kamiokande-II Collaboration and the IMB Collaboration for sharing with us their epochal data. This work was supported in part by the NSF.

Note added in proof: J. C. van der Velde (personal communication) suggests that the best estimate for the effective volume of IMB may be 6.5 ktons. This larger amount of material improves slightly the joint fits, reduces the ridge-line for the temperature by 0.2 MeV (to 3.9 MeV), and does not significantly affect the estimated fluxes.

Received 7 April; accepted 20 May 1987.

1. Hirata, K. *et al. Phys. Rev. Lett.* **58,** 1490-1493 (1987).
2. Bionata, R. M. *et al. Phys. Rev. Lett.* **58,** 1494-1496 (1987).
3. Mikheev, S. P. & Smirnov, A. Yu. *Nuovo Cimento* 9C, 17-26 (1986).
4. Wolfenstein, L. *Phys. Rev.* D17, 2369-2374 (1978).
5. Bahcall, J., Dar, A. & Piran, A. *Nature* **326,** 135-136 (1987).
6. Spergel, D. N., Piran, T., Loeb, A., Goodman, J. & Bahcall, J. N. *Phys. Rev. Lett.* (submitted).
7. Bahcall, J. *Rev. mod. Phys.* **59,** (in the press).
8. Badino, G. *et al. Nuovo Cim.* 7C, 573-590 (1984).
9. Bahcall, J. N. & Glashow, S. L. *Nature* **326,** 476-477 (1987).
10. Walker, T. P. & Schramm, D. N. *Phys. Lett.* (in the press).
11. Baade, W. & Zwicky, F. *Proc. natn. Acad. Sci.* **20,** 254-259 (1934).
12. Fowler, W. A. & Hoyle, F. *Astrophys. J. Suppl. Ser.* **9,** 201-319 (1964).
13. Colgate, S. A. & White, R. H. *Astrophys. J.* **143,** 626-681 (1966).
14. Arnett, W. D. *A. Rev. Astr. Astrophys.* **11,** 73-94 (1973).
15. Bethe, H. A. *et al. Nucl Phys.* A**324,** 487-533 (1979).
16. Bowers, R. L. & Wilson, J. R. *Astr. J. Suppl. Ser.* **50,** 115-160 (1982).
17. Arnett, W. D. *Astrophys. J.* **263,** L55-L57 (1983).
18. Bethe, H. A. & Wilson, J. R. *Astrophys. J.* **295,** 14-23 (1985).
19. Bethe, H. A. & Brown, G. *Scient. Am.* **252,** 60-68 (1985).
20. Burrows, A. & Lattimer, J. M. *Astrophys. J.* **307,** 178-196 (1985).
21. Wilson, J. R., Mayle, R., Woolsey, S. E. & Weaver, T. *Ann. N. Y. Acad. Sci.* **470,** 267-293 (1986).
22. Hayano, R. S. & Ishikawa, T. *Phys. Rev. Lett.* (submitted).
23. Hillebrant, W. *et al. Astr. Astrophys.* (submitted).

Downflows in coronal loops

R. G. Athay

High Altitude Observatory,
National Center for Atmospheric Research,
Boulder, Colorado 80307, USA

The existence of the solar wind requires a net outflow of material at all depths in the solar atmosphere. Thus, the observation of a prevalent downflow at temperatures near 10^5 K[1,2] presents a considerable challenge. Two classes of flow models have been suggested, each involving flow along closed magnetic-field lines that extend above the chromosphere into the hotter transition region and corona. Type-(1) models[3,4,5] assume unidirectional equilibrium flows along field lines and rely on asymmetry in the flow and plasma properties to produce an apparent downflow. Type-(2) models[2,6], by comparison, assume a series of episodic upflows and subsequent downflows along each line of force and rely on asymmetry in the plasma properties and flow durations to produce a statistically prevalent downflow. Here I argue that observational evidence strongly suggests that both types of flow are present but that type-(2) flow is predominant.

To establish this conclusion, we first review the observed properties of commonly occurring flows. Three features of the flow that have been extensively documented are as follows. (1) The apparent downflow velocity[1,2] reaches a maximum near 10^5 K and is markedly diminished near 2×10^5 K. (2) An upflow in the form of cool spicules[7,8] is observed near 1.5×10^4 K and has a mass flux[6,9] that agrees well with the reverse mass flux observed near 10^5 K. (3) Large-scale patterns of alternate bands of blue- and redshift separated by velocity neutral lines[10,11,12] observed near 10^5 K are well correlated with large-scale magnetic field patterns at the photospheric level, but for each magnetic neutral line there are typically two velocity neutral lines. For convenience, we refer to the former as B_0 lines and the latter as V_0 lines. In the following, we draw particular attention to the tendency for two V_0 lines to accompany each B_0 line. This observation holds an important clue to the true nature of the flow field.

It is important to note that both the velocity and magnetic maps give only the line-of-sight component of the field. Thus,